$Nd^{3+} \rightarrow Yb^{3+}$ energy transfer in the $YAl_3(BO_3)_4$ nonlinear laser crystal

D. Jaque, M. O. Ramirez, L. E. Bausá, and J. García Solé
Departamento de Física de Materiales, Facultad de Ciencias, Universidad Autónoma de Madrid, 28049 Madrid, Spain

E. Cavalli
INFM and Dipartimento di Chimica Generale ed Inorganica, Chimica Analitica e Chimica Fisica, Università di Parma, Parco Area delle Scienze 17/a, 43100 Parma, Italy

A. Speghini and M. Bettinelli
Dipartimento Scientifico e Tecnologico, University of Verona and INSTM, UdR Verona, Ca'Vignal, Strada Le Grazie 15, 37134 Verona, Italy

(Received 16 December 2002; published 30 July 2003)

The main properties of the $Nd^{3+} \rightarrow Yb^{3+}$ ($^4F_{3/2}$, $^2F_{7/2} \rightarrow {}^4I_{9/2}$, $^2F_{5/2}$) energy transfer in yttrium aluminum borate nonlinear laser crystal have been studied. This host has been found especially suitable for efficient $Nd^{3+} \rightarrow Yb^{3+}$ energy transfer because of the good matching between phonon energy and the $^4F_{3/2}(Nd^{3+})$-$^2F_{7/2}(Yb^{3+})$ energy gap ($\cong 1000\ cm^{-1}$). Energy-transfer probabilities in excess of 65% have been obtained for a Nd^{3+} (10 at. %) and Yb^{3+} (5 at. %) codoped sample. The influence of both crystal temperature and Nd^{3+} concentration on the transfer probability has been investigated. In the 15–350 K range the $Nd^{3+} \rightarrow Yb^{3+}$ energy-transfer efficiency increases with temperature, whereas for crystal temperatures above 350 K the $Nd^{3+} \leftarrow Yb^{3+}$ back transfer is activated, leading to a decrease in the effective $Nd^{3+} \rightarrow Yb^{3+}$ energy-transfer probability. The analysis of the decay curves obtained after pulsed excitation has been used to determine the multipole character of the Nd^{3+}-Yb^{3+} interaction. The donor-acceptor energy-transfer microparameter was determined [$C_{DA}(Nd^{3+} \rightarrow Yb^{3+}) \cong 18 \times 10^{-39}\ cm^6/s$], and compared to those obtained for other Nd^{3+}-Yb^{3+} co-doped materials.

DOI: 10.1103/PhysRevB.68.035118 PACS number(s): 42.55.Rz, 42.70.Hj, 42.62.Fi, 42.70.Mp

I. INTRODUCTION

Laser action in the infrared from Yb^{3+} ions shows several interesting properties when compared to the more popular Nd^{3+} ion based lasers, including the absence of excited-state absorption processes, the possibility of a certain tunability range in the IR, as well as of mode-locking operation.[1–6] Yb^{3+}-doped nonlinear crystals have recently attracted much attention as potential solid-state laser materials emitting in the green spectral domain by self-frequency doubling (SFD) of its infrared (IR) laser line ($\lambda \cong 1\ \mu m$).[7–10]

The simple energy-level diagram of Yb^{3+} provides only one possible pump channel at around $10\,000\ cm^{-1}$.[3,4] This unique pump channel does not allow the extension of the visible range covered by Yb^{3+}-doped nonlinear lasers by self-frequency sum mixing (SFSM) processes involving pump and laser radiations, as it happens for Nd^{3+} ion based nonlinear laser crystals.[11–13] For these lasers, SFSM has been successfully used because of the multiple Nd^{3+} pump channels, leading to laser generation from the ultraviolet to the green.[11–13] Therefore it would be very interesting to combine the multiple pump possibilities of Nd^{3+} ions with the good IR laser properties of Yb^{3+} ions. Thus Nd^{3+} and Yb^{3+} co-doped nonlinear crystals emerge as promising systems for tunable and pulsed laser generation in the visible domain.

Among all the rare-earth doped nonlinear crystals showing SFD in the green, Yb^{3+}-doped yttrium aluminum borate [$YAl_3(BO_3)_4$], known as Yb^{3+}:YAB, has been demonstrated to be the most efficient system (even more than Nd^{3+}:YAB).[14–17] YAB belongs to the trigonal system, space group $R32$ (huntite structure) with cell parameters $a = b = 9.295$ Å and $c = 7.243$ Å, and $Z = 3$.[18] The Y^{3+} sites, which are assumed to be occupied by both Yb^{3+} and Nd^{3+} dopant ions, have sixfold oxygen coordination and trigonal prismatic geometry with D_3 point symmetry. YAB presents a high nonlinear coefficient ($d_{eff} = 1.42\ pm\ V^{-1}$),[10] high optical quality, good mechanical strength, good thermal conductivity, chemical stability, and absence of photorefractive damage. In addition, its dispersion relations for the refractive indices allows for a broad infrared-to-visible conversion range (from the UV to the red).[11–14]

The properties of Nd^{3+} ions in YAB have been extensively studied in the past, showing interesting features such as intense absorption bands and absence of excited-state absorption.[19,20] Thus it is expected that the combination of the good properties of Yb^{3+} and Nd^{3+} ions in YAB could lead to an efficient Yb^{3+} laser oscillation under Nd^{3+} pumping via energy transfer. The potential application of this system requires a good understanding of the mechanisms involved in the energy-transfer process.

In this work we have studied the optical properties of Nd^{3+} and Yb^{3+} co-doped YAB crystals. The Yb^{3+} (acceptor) concentration was kept constant at 5 at. % (the usual Yb^{3+} concentration for efficient IR laser generation[20]) while the Nd^{3+} (donor) concentration was varied between 0.2 and 10 at. %. The variation of the donor concentration in the presence of a fixed acceptor concentration is justified because the absorption coefficient at pump wavelength (in-

creasing with donor concentration) is a crucial parameter in the optimization of the pumping efficiency.[21,22] As a consequence, the variation of energy-transfer efficiency with the donor (Nd^{3+}) concentration would be a required parameter for further modeling of the Nd^{3+}; Yb^{3+}:YAB SFSM system. The analysis of the emission spectra obtained after Nd^{3+} excitation has given detailed information on the influence of both donor concentration and crystal temperature on the $Nd^{3+} \rightarrow Yb^{3+}$ transfer efficiency. Thermally activated $Nd^{3+} \leftarrow Yb^{3+}$ back transfer has also been detected from the emission spectra obtained under Yb^{3+} excitation. Finally, the analysis of the decay curves has allowed us to determine the multipolar character of Nd^{3+}-Yb^{3+} interaction as well as to estimate the microparameter of the energy-transfer process.

II. EXPERIMENTAL DETAILS

Co-doped Nd^{3+}; Yb^{3+}:YAB crystals were grown by the flux growth method,[23] using $K_2Mo_3O_{10}+B_2O_3$ as a solvent in the 1200–700 °C temperature range, starting from reagent grade K_2CO_3 and H_3BO_3, 99.5% MoO_3, and 99.99% Y_2O_3. The dopants, substituting Y^{3+}, were added in suitable amounts as 99.99% Nd_2O_3 and Yb_2O_3. The Yb^{3+} concentration was fixed at 5 at. % whereas the Nd^{3+} concentration was varied from 0.2 to 10 at. % (0.2, 2, 4, 6, and 10 at. %). Good optical quality crystals with a size of about $1\times1\times3\ mm^3$ were obtained. Larger YAB crystals up to about $20\times12\times10\ mm^3$ in size can be grown by means of the top seeded solution growth technique (TSSG),[10] not available in our laboratory.

For continuous-wave fluorescence spectra a 0.6-W fiber coupled diode tuned to 807 nm and an argon pumped Ti:sapphire laser (Spectra Physics, model 3900) tuned to 980 nm were used. The emission experiments under pulsed excitation were performed by using an optical parametric oscillator (OPO Quanta Ray) which provides 10-ns pulses with an average energy of 10 mJ. OPO wavelength was 520 and 975 nm for Nd^{3+} and Yb^{3+} excitation, respectively. The luminescence was dispersed by a 500 M SPEX monochromator and detected with a calibrated Ge detector or a cooled photomultiplier. In continuous-wave fluorescence experiments the signals were recorded by using an EG&G lock-in amplifier. Decay time measurements were performed using a Tektronix 2400 digital storage oscilloscope. Temperature was varied between 15 and 600 K by mounting the samples in a Leybold temperature-controlled closed-He-cycle cryostat.

Finally, Raman measurements were carried out using a small optically polished single crystal. The 488.0-nm line of a Spectra-Physics Stabilite 2017 argon laser was used to obtain room-temperature Raman spectra. A fiber-optic probe coupled to a Dilor Superhead, equipped with a suitable notch filter, was employed. The scattered signal was analyzed by a Jobin-Yvon HR460 monochromator and a charge-coupled device (CCD) detector. Spectra were collected using a 1200-lines/mm grating with a spectral resolution of about 1 cm^{-1}.

III. RESULTS AND DISCUSSION

A. Suitability of YAB lattice for efficient $Nd^{3+} \rightarrow Yb^{3+}$ energy transfer

Figure 1 shows the schematic energy-level diagrams of Nd^{3+} and Yb^{3+} ions in YAB. As for other Nd^{3+}; Yb^{3+} co-doped crystals and glasses there is an energy gap ΔE between the $^4F_{3/2}$ (Nd^{3+}) and $^2F_{5/2}$ (Yb^{3+}) metastable excited states. As a consequence, resonant energy transfer is not possible. Nevertheless, energy transfer between trivalent neodymium and ytterbium ions has been reported in several crystalline and glass hosts and attributed to the $^4F_{3/2}$, $^2F_{7/2} \rightarrow {}^2I_{9/2}$, $^2F_{5/2}$ phonon-assisted process.[24,25] The Dexter model,[26] widely used to characterize the resonant energy transfer, predicts a linear relationship between the transfer probability (W_t) and the spectral overlap between donor emission and acceptor absorption bands, so that[26]

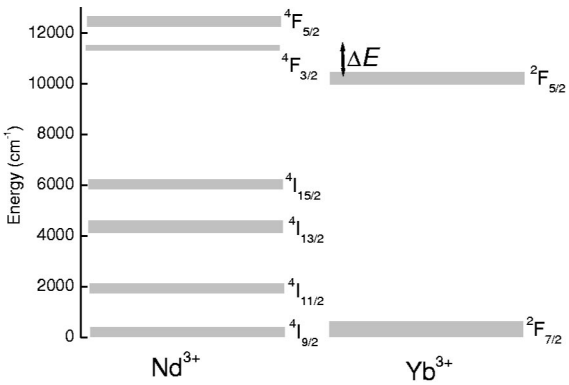

FIG. 1. Schematic energy-level diagram of Nd^{3+} and Yb^{3+} ions.

$$W_t \propto \int \frac{f_d(E) f_a(E)}{E^2} dE, \tag{1}$$

where $f_a(E)$ and $f_d(E)$ are the line-shape functions of the acceptor absorption and donor emission cross sections, respectively. Figure 2(a) shows the unpolarized room-temperature emission cross section of Nd^{3+} ions ($^4F_{3/2} \rightarrow {}^4I_{9/2}$) and the Yb^{3+} absorption ($^2F_{7/2} \rightarrow {}^2F_{5/2}$) cross section in YAB. The spectra shown in Fig. 2(a) were obtained from singly (Nd^{3+} or Yb^{3+}) doped YAB crystals. As can be observed, spectral overlap is negligible and efficient $Nd^{3+} \rightarrow Yb^{3+}$ energy transfer requires the participation of one or more phonons. The Dexter model can be easily generalized to the nonresonant phonon-assisted energy-transfer case by taking into account the energy of the phonon involved (E_{ph}) as well as the phonon density.[27] If we assume that only one phonon is involved,

$$W_t \propto I(E_{ph}) = \frac{e^{E_{ph}/kT}}{e^{E_{ph}/kT}-1} \int \frac{f_d(E-E_{ph}) f_a(E)}{E^2} dE, \tag{2}$$

where $I(E_{ph})$ is here defined as the phonon-assisted overlap.

By using the cross-section spectra of Fig. 2(a) we have calculated the $I(E_{ph})$ function at room temperature for phonon energies up to 1400 cm^{-1}. Results are shown in Fig. 2(b) (dotted line). The unpolarized Raman spectrum of YAB is also shown in this figure (solid line). The maximum phonon-assisted overlap is obtained for phonon energies of about 1070 cm^{-1}, very close to the most intense Raman mode of YAB (1030 cm^{-1}). Thus, in the case of YAB, Nd^{3+}-Yb^{3+}

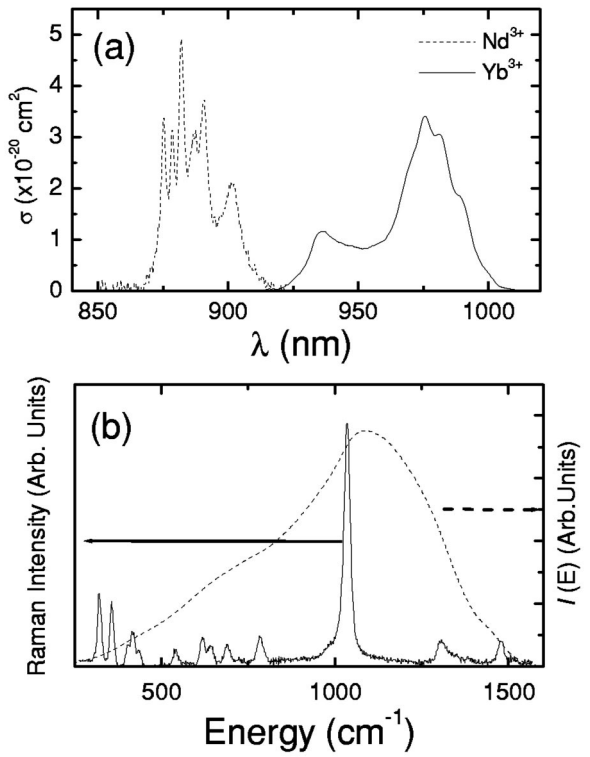

FIG. 2. (a) Nd^{3+} emission and Yb^{3+} absorption cross section. (b) Phonon-assisted overlap $I(E_{ph})$ as a function of phonon energy (dotted line). Room-temperature Raman spectrum of YAB (solid line).

energy-level mismatch can be efficiently covered by the single emission of one of these phonons although the participation of phonons with other energies cannot be completely disregarded. This coincidence strongly suggests that YAB crystal is a good candidate for efficient Nd^{3+}-Yb^{3+} energy transfer.

B. Determination of the energy-transfer efficiency: Influence of Nd^{3+} concentration

Figure 3 shows the room-temperature unpolarized emission spectra obtained for all the Nd^{3+} concentrations used in this work. Excitation was made by a laser diode tuned to 807 nm. In order to avoid local crystal heating and up-conversion processes we used a pump power of 20 mW. All the spectra shown in Fig. 3 were normalized to the value obtained at 890 nm (a wavelength within the $^4F_{3/2} \rightarrow {}^4I_{9/2}$ Nd^{3+} emission). The broad emission range (from 850 to 1120 nm) is due to both Nd^{3+} ($^4F_{3/2} \rightarrow {}^4I_{9/2}$ and $^4F_{3/2} \rightarrow {}^4I_{11/2}$) and Yb^{3+} ($^2F_{5/2} \rightarrow {}^2F_{7/2}$) transitions. Thus Fig. 3 is a clear evidence of the existence of an efficient $Nd^{3+} \rightarrow Yb^{3+}$ energy transfer. As we will see in Sec. III D, the reduction in the Nd^{3+} fluorescence lifetime caused by the $Nd^{3+} \rightarrow Yb^{3+}$ transfer rate indicates a nonradiative mechanism. It can be also observed in Fig. 3 how the Yb^{3+} emission intensity increases with the Nd^{3+} concentration.

From the data displayed in Fig. 3 it is possible to determine the energy-transfer efficiency for each Nd^{3+} concentration. If we denote as n_{Nd_1}, n_{Nd_2}, n_{Yb_1}, and n_{Yb_2} the population densities of the $^4I_{9/2}$, $^4F_{3/2}$, $^2F_{7/2}$, and $^2F_{5/2}$ states, respectively (see Fig. 1), the rate equations governing the level populations of these states are

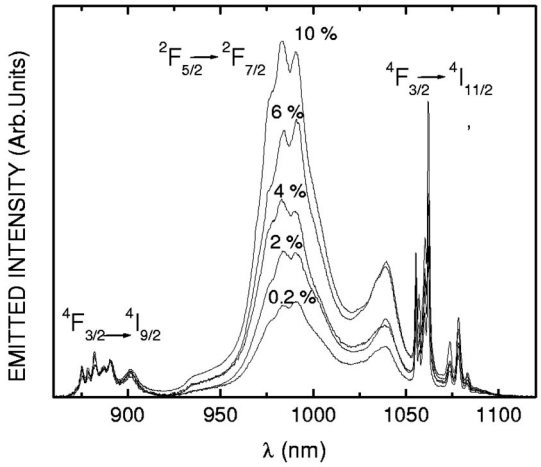

FIG. 3. Room-temperature emission spectra obtained from all the samples used in the present work. The pump wavelength was 807 nm.

$$\frac{dn_{Nd_1}}{dt} = -Pn_{Nd_1} + (W_{Nd}^{nr} + W_{Nd}^{r})n_{Nd_2} + W_t n_{Nd_2} n_{Yb_1} - W_{bt} n_{Nd_1} n_{Yb_2} = -\frac{dn_{Nd_2}}{dt}, \tag{3}$$

$$\frac{dn_{Yb_1}}{dt} = (W_{Yb}^{nr} + W_{Yb}^{r})n_{Yb_2} + W_{bt} n_{Nd_1} n_{Yb_2} - W_t n_{Nd_2} n_{Yb_1} = -\frac{dn_{Yb_2}}{dt}, \tag{4}$$

where P is the optical pump rate, $W_{Nd}^{r} + W_{Nd}^{nr}$ is the total de-excitation rate of Nd^{3+} excited ions in the absence of energy transfer (W_{Nd}^{r} and W_{Nd}^{nr} being the Nd^{3+} radiative and nonradiative decay probabilities, respectively), $W_{Yb}^{r} + W_{Yb}^{nr}$ is the total de-excitation probability of Yb^{3+} excited ions in the absence of energy transfer (W_{Yb}^{r} and W_{Yb}^{nr} being the Yb^{3+} radiative and nonradiative decay probabilities, respectively), W_t is the $Nd^{3+} \rightarrow Yb^{3+}$ energy-transfer term and W_{bt} is the $Nd^{3+} \leftarrow Yb^{3+}$ back-transfer term. As we will see in next section, back transfer at room temperature (RT) can be considered negligible with respect to $Nd^{3+} \rightarrow Yb^{3+}$ transfer ($W_{bt} \ll W_t$ at RT). Under these conditions, the energy-transfer efficiency η_t (defined as the number of Nd^{3+} ions de-excited via Yb^{3+} emission divided by the total number of Nd^{3+} ions de-excited per unit of time) can be written as

$$\eta_t = \frac{W_t n_{Yb_1}}{W_{Nd}^{r} + W_{Nd}^{nr} + W_t n_{Yb_1}}. \tag{5}$$

The number of Yb^{3+} ions excited per unit of time due to the $Nd^{3+} \rightarrow Yb^{3+}$ transfer is given by $n_{Nd_2} W_t n_{Yb_1}$. This can be evaluated from the emission spectra, which is taken under continuous excitation:[28]

$$n_{Nd_2} W_t n_{Yb_1} = \frac{\alpha}{\eta_{Yb}} \int_{850\ nm}^{1100\ nm} I_{lum}^{Yb}(\lambda) d\lambda, \quad (6)$$

where I_{lum}^{Yb} is the luminescence intensity of wavelength λ emitted by Yb^{3+} ions, η_{Yb} is the fluorescence quantum efficiency of the $^2F_{5/2}$ state [$\eta_{Yb} \approx 0.9$ (Ref. 10)] and α is a constant which includes the mean emission wavelength as well as the absolute spectral response of the experimental setup. As we will see the evaluation of this constant is not necessary for determining the energy-transfer efficiency.

Previous studies have determined that the fluorescence quantum efficiency of the metastable state of Nd^{3+} ions in YAB, η_{Nd}, is as low as 0.18.[19,29] As a consequence,

$$\eta_{Nd} = \frac{W_{Nd}^r}{W_{Nd}^r + W_{Nd}^{nr}} \approx 0.2 \Rightarrow W_{Nd}^r + W_{Nd}^{nr} \approx 5.6 W_{Nd}^r. \quad (7)$$

The radiative rate of Nd^{3+} ions, W_{Nd}^r, can be also obtained from the contribution of Nd^{3+} ions to the emission spectra shown in Fig. 3. For this purpose, it is important to take into account that both $^4F_{3/2} \rightarrow {}^4I_{13/2}$ and $^4F_{3/2} \rightarrow {}^4I_{15/2}$ Nd^{3+} emission bands (located at 1.3 and 1.8 μm, respectively) have not been recorded. The branching ratios corresponding to the four transitions originating from the $^4F_{3/2}$ metastable state have been previously reported [$\beta_{^4I_{9/2}} + \beta_{^4I_{11/2}} \approx 9 \beta_{^4I_{13/2}}$ and $\beta_{^4I_{15/2}} \approx 0$ (Ref. 19)]. As a consequence,[28]

$$W_{Nd}^r + W_{Nd}^{nr} = 5.6 W_{Nd}^r = \frac{5.6\alpha}{n_{Nd_2}} \int_{850\ nm}^{2000\ nm} I_{lum}^{Nd}(\lambda) d\lambda$$

$$= \frac{6.2\alpha}{\eta_{Nd_2}} \int_{850\ nm}^{1100\ nm} I_{lum}^{Nd}(\lambda) d\lambda, \quad (8)$$

where $I_{lum}^{Nd}(\lambda)$ is the luminescence intensity of wavelength λ emitted by Nd^{3+} ions, α is the coupling constant, which is assumed to be the same as that of expression (6) since the Nd^{3+} and Yb^{3+} emissions considered here occur in the same spectral range (similar mean emission wavelengths). Combining Eqs. (5), (6), and (8) the transfer efficiency can be expressed as

$$\eta_t = \frac{1.1 \int_{850\ nm}^{1100\ nm} I_{lum}^{Yb}(\lambda) d\lambda}{6.2 \int_{850\ nm}^{1100\ nm} I_{lum}^{Nd}(\lambda) d\lambda + 1.1 \int_{850\ nm}^{1100\ nm} I_{lum}^{Yb}(\lambda) d\lambda} \quad (9)$$

so that the evaluation of the coupling constant α is no longer necessary.

Figure 4 shows the dependence of transfer efficiency on Nd^{3+} concentration obtained by applying expression (9) to the room-temperature emission spectra shown in Fig. 3. The $Nd^{3+} \rightarrow Yb^{3+}$ energy-transfer efficiency increases with Nd^{3+} (donor) concentration (from 0.40 up to 0.65 when the Nd^{3+} content is increased from 0.2 to 10 at. %). This behavior could be in principle attributed to the decrease in the average Nd^{3+}-Yb^{3+} distance, d, caused by the increment in donor concentration. As a matter of fact, this distance is usually estimated by $d = [3/4\pi N]^{1/3}$ where N is the total (acceptor + donor) density of ions (both Nd^{3+} and Yb^{3+} ions occupy the same Y^{3+} lattice site).[25]

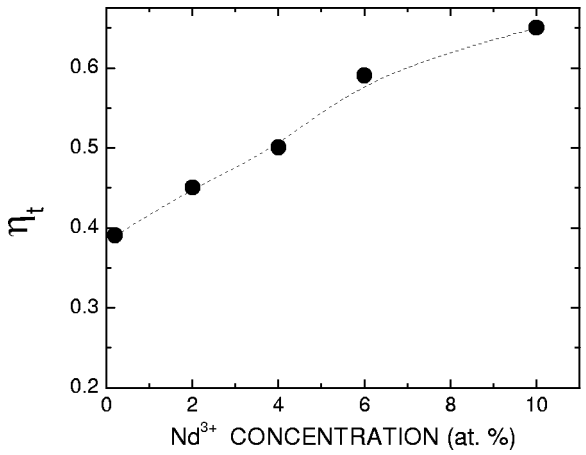

FIG. 4. $Nd^{3+} \rightarrow Yb^{3+}$ room-temperature energy-transfer efficiency as a function of Nd^{3+} concentration. Dots are experimental data obtained from emission spectra and the dotted line is a guide for the eyes.

The values obtained for energy-transfer efficiency can be compared with those reported for $YAlO_3$ ($\eta_t = 0.79$ for 1 and 2 at. % of Nd^{3+} and Yb^{3+}, respectively),[24] for $NaGdWO_4$ ($\eta_t = 0.58$ for 2 and 2 at. % of Nd^{3+} and Yb^{3+}, respectively),[30] for $Ba_2MgGe_2O_7$ ($\eta_t = 0.2$ for 2 and 2 at. % of Nd^{3+} and Yb^{3+}, respectively)[31] and for $LiYF_4$ ($\eta_t = 0.58$ for 2 and 2 at. % of Nd^{3+} and Yb^{3+}, respectively).[32] Due to the differences in the crystal structures and in the Nd^{3+} and Yb^{3+} concentrations, a direct quantitative comparison of these values is not possible. Nevertheless, it is reasonable to say that the transfer efficiency obtained in our most concentrated sample ($\eta_t = 0.65$) is among the highest values reported for Nd^{3+}-Yb^{3+} co-doped crystals. This ensures an efficient population of excited Yb^{3+} ions under direct excitation of Nd^{3+} ions.

C. Influence of crystal temperature: Evidence of thermally activated $Nd^{3+} \leftarrow Yb^{3+}$ back transfer

The low quantum efficiency of the $^4F_{3/2}$ metastable state of Nd^{3+} ions in YAB [$\eta_{Nd} \approx 0.18$ (Refs. 19, 29)] is a consequence of a large nonradiative decay probability from the metastable state. As a consequence, under high or moderate pump intensities a strong pump induced crystal heating is observed in Nd^{3+}:YAB laser crystals.[33,34] The thermal loading caused by pump radiation depends on several factors such as pump wavelength, pump geometry, and on the presence/absence of stimulated emission.[35] For pump powers of 1 W crystal temperatures above 100 °C have been reported in a diode pumped Nd^{3+}:YAB laser crystal oscillating at 1.062 μm.[34,35] This pump induced crystal heating would be also present in a Nd^{3+}; Yb^{3+}:YAB laser system pumped through Nd^{3+} ions. Therefore it is necessary to get a further understanding on the influence of temperature in the $Nd^{3+} \rightarrow Yb^{3+}$ transfer efficiency.

Figure 5 shows the unpolarized emission spectra obtained from the Nd^{3+} (10 at. %); Yb^{3+} (5 at. %):YAB sample at

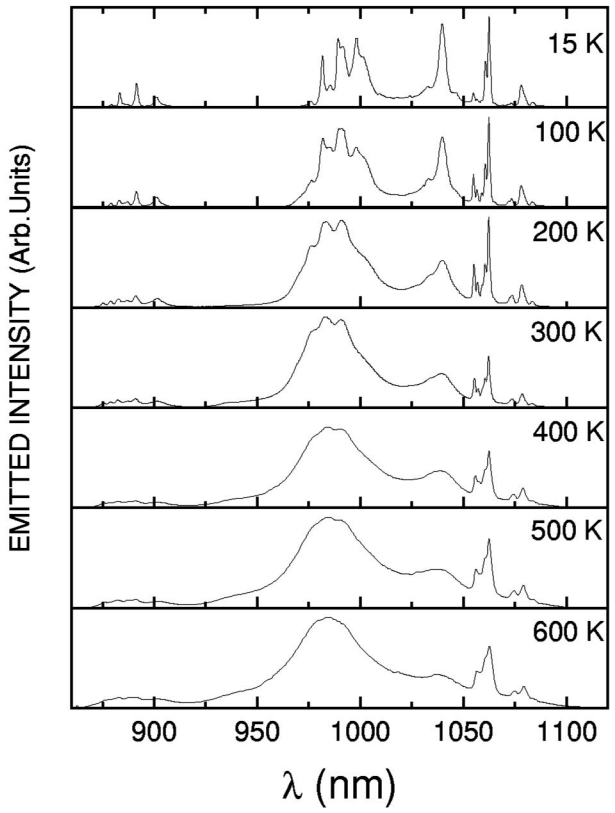

FIG. 5. Temperature dependence of the unpolarized emission spectra obtained from the Nd^{3+} (10 at. %) and Yb^{3+} (5 at. %) co-doped YAB sample. The pump wavelength was 807 nm.

different temperatures, with an excitation wavelength of 807 nm. Special care was taken in order to avoid pump induced local heating of the YAB crystal. It is clear that $Nd^{3+} \rightarrow Yb^{3+}$ transfer is taking place in all the temperature range under investigation (from 15 to 600 K). From data displayed in Fig. 5 it is possible to estimate, in a first-order approximation, the temperature dependence of the $Nd^{3+} \rightarrow Yb^{3+}$ energy-transfer efficiency by applying Eq. (9). Results obtained are shown in Fig. 6. A nonmonotonic behavior is obtained. In the 15–350-K range the transfer efficiency increases with temperature. A further increment in the crystal temperature produces a significant decrease in the transfer efficiency. The net $Nd^{3+} \rightarrow Yb^{3+}$ transfer efficiency can change with temperature because of different causes. These are: (i) modifications in the population distribution among the Stark levels leading to changes in the spectral profiles of the Nd^{3+} and Yb^{3+} bands, (ii) thermally induced line broadening of emission and absorption bands, (iii) changes in the probability of phonon-assisted processes (changes in the assisting phonon density), and (iv) thermally activated $Nd^{3+} \leftarrow Yb^{3+}$ back transfer. The relative importance of these effects determines the final temperature dependence of the energy-transfer efficiency. However, the quantitative evaluation of these effects is complicated and lies outside the scope of this paper. The transfer efficiency behavior in the 15–350-K range seems to be determined by the increase of the assisting phonon density. As we will see, thermally activated

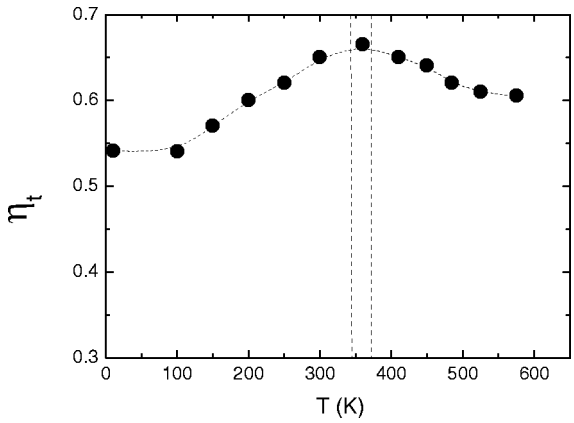

FIG. 6. Temperature dependence of the $Nd^{3+} \rightarrow Yb^{3+}$ energy-transfer efficiency as obtained from emission spectra. Dots are the experimental data obtained from the Nd^{3+} (10 at. %) and Yb^{3+} (5 at. %) co-doped YAB sample and the dotted line is a guide for the eyes.

$Nd^{3+} \leftarrow Yb^{3+}$ back transfer causes the decrease of transfer efficiency for temperatures above 350 K.

In order to check the presence of $Nd^{3+} \leftarrow Yb^{3+}$ back transfer we have performed emission experiments by exciting the sample at 945 nm (Yb^{3+} ions excitation). In the absence of $Nd^{3+} \leftarrow Yb^{3+}$ energy transfer, the emission spectrum should be composed only of the emissions corresponding to the ${}^2F_{7/2} \rightarrow {}^2F_{5/2}$ (Yb^{3+}) transition (broad band centered around 1 μm). The activation of $Nd^{3+} \leftarrow Yb^{3+}$ energy transfer would be detected by the presence of Nd^{3+} bands in the emission spectrum (at 0.89 and 1.06 μm). Figure 7 shows the unpolarized emission spectra obtained from the Nd^{3+} (10 at. %); Yb^{3+} (5 at. %):YAB sample at 15, 300, and 600 K. From this figure it is clear that Nd^{3+} emission bands (marked by arrows) are only appreciable when the crystal temperature is above 300 K, this being a clear evidence of the temperature activated $Nd^{3+} \leftarrow Yb^{3+}$ energy back transfer. Following the same arguments as in Sec. III B), the $Nd^{3+} \leftarrow Yb^{3+}$ back transfer efficiency η_{bt} can be calculated from emission spectra by

$$\eta_{bt} = \frac{6.2 \int_{850\ nm}^{1100\ nm} I_{lum}^{Nd}(\lambda) d\lambda}{6.2 \int_{850\ nm}^{1100\ nm} I_{lum}^{Nd}(\lambda) d\lambda + 1.1 \int_{850\ nm}^{1100\ nm} I_{lum}^{Yb}(\lambda) d\lambda}. \quad (10)$$

We have calculated the temperature dependence of the $Nd^{3+} \leftarrow Yb^{3+}$ back transfer efficiency by measuring the unpolarized emission spectra in the 800–1100-nm range under Yb^{3+} excitation (these spectra are not shown for the sake of brevity). The results are shown in Fig. 8. Due to the requirement of phonon annihilation (absorption), $Nd^{3+} \leftarrow Yb^{3+}$ transfer is only appreciable when the temperature is raised above 350 K. As a consequence, it is now clear that the decrease in the net $Nd^{3+} \rightarrow Yb^{3+}$ transfer efficiency for temperatures above 350 K is related to thermally activated $Nd^{3+} \leftarrow Yb^{3+}$ back transfer which produces an overall reduction (increment) in the Yb^{3+} (Nd^{3+}) steady-state population. Data shown in Fig. 6 indicates that in a Nd^{3+};

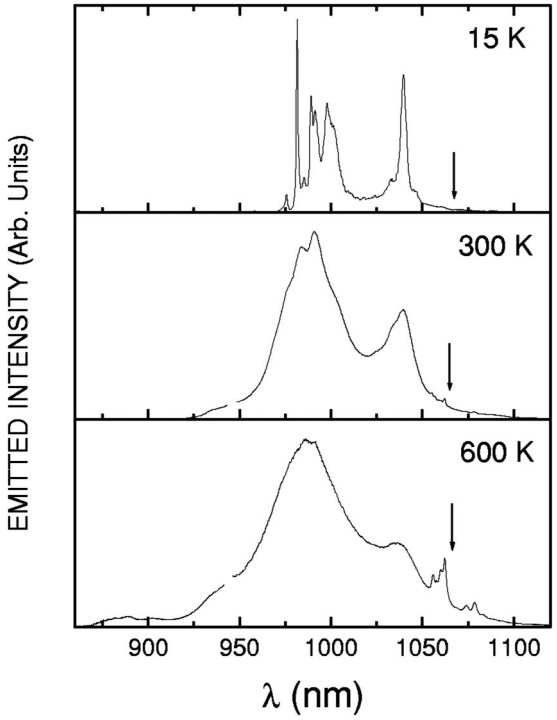

FIG. 7. Unpolarized emission spectra obtained from the Nd^{3+} (10 at. %) and Yb^{3+} (5 at. %) co-doped YAB sample at 15, 300, and 600 K. The pump wavelength was 945 nm. Arrows indicate the spectral position of Nd^{3+} emission. The laser line has been removed.

Yb^{3+}:YAB laser operating at the Yb^{3+} emission through Nd^{3+} pumping, thermal control and stabilization of gain medium is required for efficient and stable pumping efficiency.

D. Analysis of the decay curves

In this section the decay curves obtained under pulsed excitation are analyzed in order to determine some important parameters of the $Nd^{3+} \rightarrow Yb^{3+}$ energy transfer such as the nature of the Nd^{3+}-Yb^{3+} coupling and the energy-transfer microparameter. Furthermore, lifetime measurements are also used to determine the radiative or nonradiative mechanism of the $Nd^{3+} \rightarrow Yb^{3+}$ energy transfer.

Figure 9 shows the decay curves of the room-temperature luminescence of Nd^{3+} ions from the $^4F_{3/2}$ state (monitored at 890 nm) obtained for all the Nd^{3+} concentrations used in this work. As can be observed the decay curves are strongly dependent on the Nd^{3+} (donor) concentration. In addition to the method described in Sec. III B), the transfer efficiency can be also calculated from decay time experiments by[25,36]

$$\eta_t = 1 - \frac{\tau_{\text{Nd-Yb}}}{\tau_{\text{Nd}}}, \tag{11}$$

where τ_{Nd} and $\tau_{\text{Nd-Yb}}$ are the $^4F_{3/2}$ fluorescence lifetime obtained for Nd^{3+} and Nd^{3+};Yb^{3+} co-doped samples (with the same Nd^{3+} concentration), respectively. Figure 10(a) shows the concentration dependence of $\tau_{\text{Nd-Yb}}$ (here defined as the time at which the fluorescence intensity has decayed to e^{-1} of its initial value). The variation of the $^4F_{3/2}$ fluorescence lifetime with concentration for singly doped Nd^{3+} crystals τ_{Nd} is given by[33]

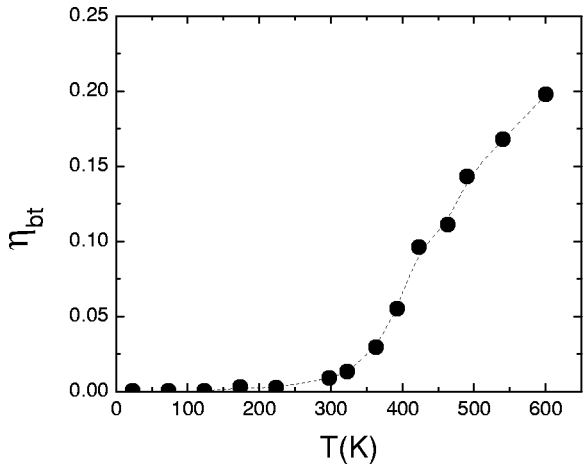

FIG. 8. Temperature dependence of the back transfer efficiency calculated from emission spectra. Dots are experimental data obtained from Nd^{3+} (10 at. %) and Yb^{3+} (5 at. %) co-doped YAB sample and the dotted line is a guide for the eyes.

$$\tau_{\text{Nd}} = \frac{60\ \mu\text{s}}{1 + 0.02 n_{\text{Nd}}}, \tag{12}$$

where n_{Nd} is the total Nd^{3+} concentration in the crystal in at. % units. The concentration dependence of Nd^{3+} fluorescence lifetime [as obtained from Eq. (12)] is also shown in Fig. 10(a) (full line). It is then possible to determine the energy-transfer efficiency as a function of donor concentration. The values for η_t obtained from expressions (11) and (12) are represented in Fig. 10(b). There is a good agreement between energy-transfer efficiencies obtained from emission

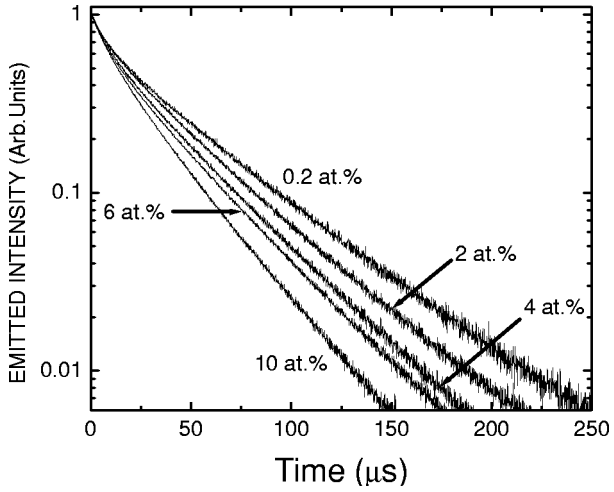

FIG. 9. Time evolution of the room-temperature Nd^{3+} fluorescence obtained for all the samples used in this work.

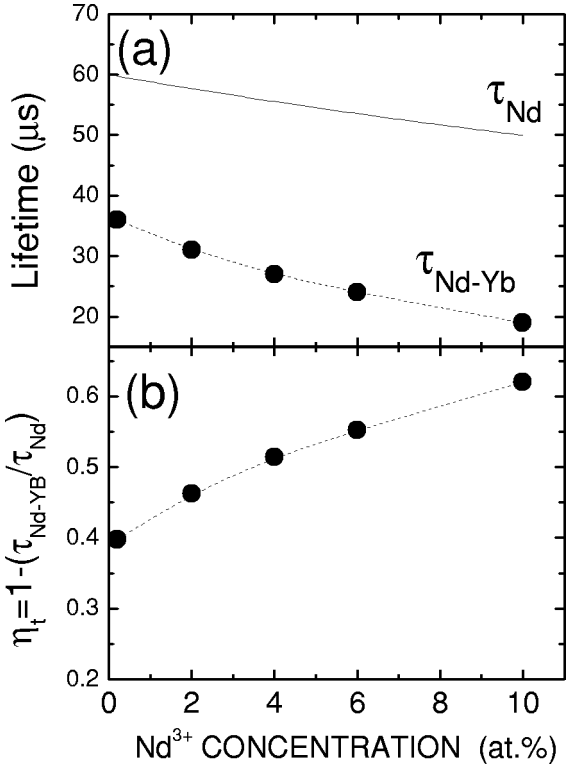

FIG. 10. (a) Room temperature Nd^{3+} lifetime as a function of Nd^{3+} concentration in the presence ($\tau_{Nd\text{-}Yb}$: solid circles) and absence (τ_{Nd}: solid line) of Yb^{3+} ions. (b) $Nd^{3+} \rightarrow Yb^{3+}$ transfer efficiency calculated from data displayed in Fig. 10(a). The dotted lines are guides for the eyes.

spectra and those calculated from decay time measurements [see Figs. 4 and 10(b)]. This good agreement indicates that, if radiative energy transfer is taking place, its contribution to the total $Nd^{3+} \rightarrow Yb^{3+}$ transfer can be considered negligible (radiative energy transfer does not cause any reduction in donor lifetime[28]).

The decay curves shown in Fig. 9 are clearly nonexponential. According to previous models the time dependence of donor luminescence following a short excitation may be written as[37–41]

$$I(t) = I_0 \exp\left[-\frac{t}{\tau_0} - \pi(t) \right] = I_0 \exp[-\alpha t - \pi(t)], \quad (13)$$

where τ_0 is the intrinsic lifetime of donor ions, t is the time after excitation, and the function $\pi(t)$ describes the effects of interactions involving both Nd^{3+} and Yb^{3+} ions, i.e., excitation energy migration over donors, self-quenching of donor luminescence, and excitation energy transfer to acceptors. The time dependence of $\pi(t)$ depends on the multipolar donor-acceptor (Nd^{3+}-Yb^{3+}) couplings. When energy migration over donors may be neglected, $\pi(t)$ has a Förster-like time dependence:[41,42]

$$\pi(t) = \gamma_S t^{3/S}, \quad (14)$$

where γ_S is a time independent constant and $S=6$, 8, and 10 stands out for dipole-dipole, dipole-quadrupole, and quadrupole-quadrupole interactions. Since energy migration between donors has been neglected in expression (14), it could only be applied to the decay curves obtained from the sample with the lowest donor (Nd^{3+}) concentration (0.2 at. %). Figure 11 shows the time dependence of the Nd^{3+} fluorescence obtained from the 0.2-at. %-doped sample. Open circles are experimental data and solid lines are the best fits to Eqs. (13) and (14) by assuming dipole-dipole ($S=6$), dipole-quadrupole ($S=8$), and quadrupole-quadrupole ($S=10$) couplings. The best agreement between experimental data and theoretical fit is obtained for $S=6$. These results indicate that the dipole-dipole interaction is dominant in the energy-transfer process. Nevertheless, some contribution of the dipole-quadrupole interaction cannot be disregarded. This conclusion is in agreement with the Nd^{3+}-Yb^{3+} interaction character observed in other Nd^{3+}-Yb^{3+} co-doped hosts.[25,37] Once the main multipolar character has been determined it is then possible to estimate the donor-acceptor microparameter for the Nd^{3+}-Yb^{3+} interaction $C_{DA}^{Nd\text{-}Yb}$. For a dipole-dipole interaction the $Nd^{3+} \rightarrow Yb^{3+}$ energy-transfer microparameter is given by[40–42]

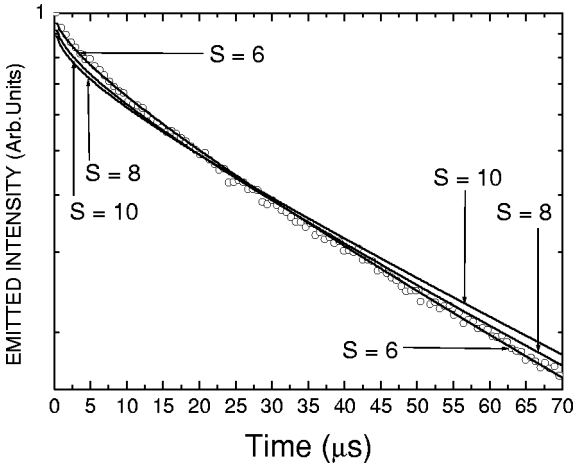

FIG. 11. Room-temperature time dependence of Nd^{3+} emission obtained for the Nd^{3+} (0.2 at. %) and Yb^{3+} (5 at. %) co-doped YAB sample. Open circles are experimental data and solid lines are the best fits to expression (13) for a dipole-dipole ($S=6$), dipole-quadrupole ($S=8$), and quadrupole-quadrupole coupling ($S=10$).

$$\gamma_6^{Nd\text{-}Yb} = \tfrac{4}{3}\pi^{3/2}\rho_A\sqrt{C_{DA}^{Nd\text{-}Yb}}, \quad (15)$$

where ρ_A is the acceptor density. From the fitting of Fig. 11 to expression (14) a value of $\gamma_6^{Nd\text{-}Yb} \approx 0.80\times10^3\ s^{-1/2}$ has been obtained. Then, by using expression (15) we have obtained $C_{DA}^{Nd\text{-}Yb} = 18\times10^{-39}\ cm^6\ s^{-1}$. This value is higher than $C_{DA}^{Nd\text{-}Yb} = 3.8\times10^{-39}$, 2.4×10^{-39}, 0.34×10^{-39}, 1.6×10^{-39}, and $6.0\times10^{-39}\ cm^6\ s^{-1}$ obtained for tellurite,[37] Pb-ultraphosphate,[37] fluoroindogallate,[25] metaphosphate,[43] and borate glasses.[44] Among all the values reported for the $C_{DA}^{Nd\text{-}Yb}$ parameter, the highest have been obtained in borate compounds (crystals and glasses). This fact can be related to the high-energy phonons associated with the (BO_3) group, so that the number of phonons required to cover the energy

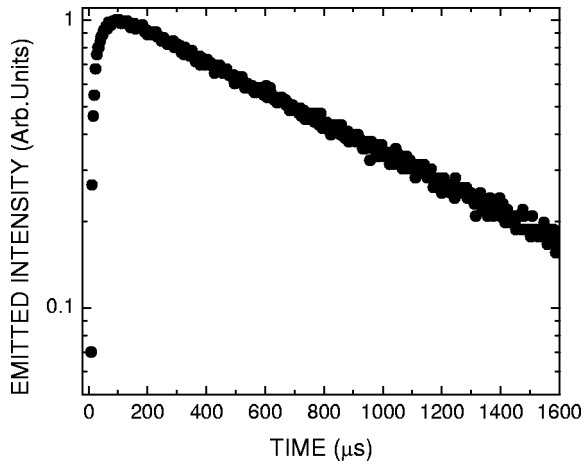

FIG. 12. Room-temperature time dependence of Yb^{3+} emission obtained for the Nd^{3+} (10 at. %) and Yb^{3+} (5 at. %) co-doped YAB sample. The pump wavelength was 520 nm.

gap between Nd^{3+} and Yb^{3+} excited levels is 1. Furthermore, the fact that in the particular case of YAB crystals the microparameter of energy transfer is higher than those obtained for other matrices could be related to the coincidence between the Nd^{3+}-Yb^{3+} energy gap and the energy of the most intense Raman phonon (see Fig. 2).

The temporal evolution of Yb^{3+} ($^2F_{5/2}$) luminescence after Nd^{3+} ions excitation has been also recorded. Figure 12 shows the room temperature Yb^{3+} fluorescence decay curve obtained from the 10-at. % Nd^{3+}-co-doped sample under 0.52-μm excitation. As can be observed, the Yb^{3+} fluorescence intensity exhibits an initial transient buildup at a rate corresponding to excitation via transfer from Nd^{3+} ions. After this initial buildup ($\tau_{up} \approx 20\ \mu s$), the Yb^{3+} fluorescence exhibits a simple exponential time dependence. The characteristic time for this decay $\tau_{Nd\text{-}Yb}$ for the crystal containing 10 at. % of Nd^{3+} and 5 at. % of Yb^{3+} is plotted as a function of temperature in Fig. 13(a). The temperature dependence of the Yb^{3+} lifetime in the presence of Nd^{3+} ions can be also used to determine the $Nd^{3+} \leftarrow Yb^{3+}$ back transfer efficiency η_{bt} by

$$\eta_{bt} = 1 - \frac{\tau_{Nd\text{-}Yb}}{\tau_{Yb}}, \tag{16}$$

where $\tau_{Nd\text{-}Yb}$ is the lifetime of the $^2F_{5/2}$ level of Yb^{3+} in the presence of Nd^{3+} ions and τ_{Yb} is the fluorescence lifetime of the $^2F_{5/2}$ level of Yb^{3+} in the absence of Nd^{3+} ions. The temperature dependence of τ_{Yb} has been measured for a 5-at. % singly doped Yb^{3+}:YAB crystal under 975 nm excitation. Results are also shown in Fig. 13(a). As can be observed, the behavior of $\tau_{Nd\text{-}Yb}$ and τ_{Yb} is very similar up to 300 K. For higher temperatures $\tau_{Nd\text{-}Yb} < \tau_{Yb}$, indicating the presence of thermally activated back transfer. The back transfer efficiency as a function of temperature is displayed in Fig. 13(b). A reasonable good agreement with the values obtained from the emission spectra (see Figs. 7 and 8) is observed. As for the case of $Nd^{3+} \rightarrow Yb^{3+}$ transfer, this agreement indicates that the presence of $Nd^{3+} \leftarrow Yb^{3+}$ radiative energy transfer can be neglected.

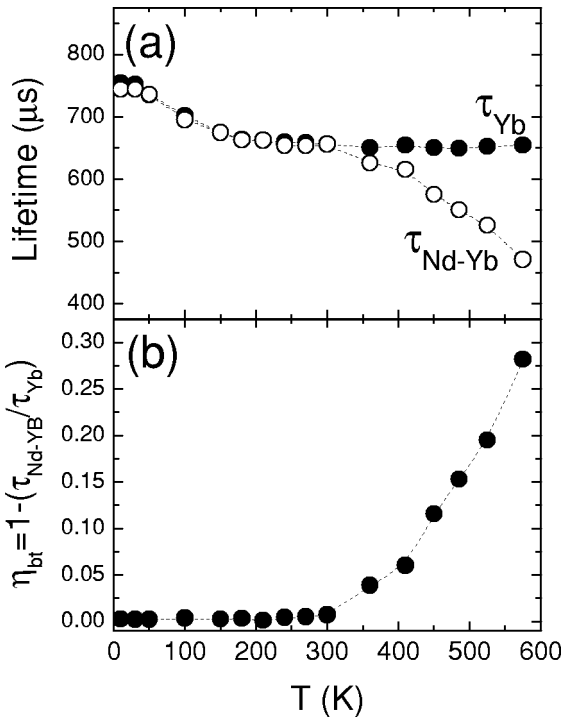

FIG. 13. (a) Yb^{3+} lifetime as a function of temperature in the presence ($\tau_{Nd\text{-}Yb}$: open circles) and absence (τ_{Yb}: solid circle) of Nd^{3+} ions. (b) $Nd^{3+} \leftarrow Yb^{3+}$ back transfer efficiency (η_{bt}) calculated from lifetime values. The dotted lines are guides for the eyes.

IV. CONCLUSIONS

$Nd^{3+} \rightarrow Yb^{3+}$ energy transfer in co-doped yttrium aluminum borate crystals has been demonstrated. The main properties of the ($^4F_{3/2}$, $^2F_{7/2} \rightarrow {}^4I_{9/2}$, $^2F_{5/2}$) $Nd^{3+} \rightarrow Yb^{3+}$ energy transfer have been systematically studied as a function of Nd^{3+} (donor) concentration and crystal temperature. Emission spectra obtained under both Nd^{3+} and Yb^{3+} excitation in the 800–1200-nm range have been used to determine the transfer ($Nd^{3+} \rightarrow Yb^{3+}$) and back-transfer ($Nd^{3+} \leftarrow Yb^{3+}$) efficiencies. The transfer efficiency has been found to be enhanced by increasing the donor concentration, being, at room temperature, as high as 0.65 for the most concentrated crystals (10 and 5 at. % of Nd^{3+} and Yb^{3+} ions, respectively). It has been demonstrated that when crystal temperature is increased above 350 K the $Nd^{3+} \leftarrow Yb^{3+}$ transfer is activated leading to a reduction in the net $Nd^{3+} \rightarrow Yb^{3+}$ energy-transfer efficiency. The decay curves obtained at room temperature have been used to conclude that a predominant electric dipole-dipole character for the $Nd^{3+}Yb^{3+}$ coupling is taking place. In addition, we have also evaluated the donor-acceptor microparameter of energy transfer ($C_{DA}^{Nd\text{-}Yb} \cong 18 \times 10^{-39}$ cm^6/s). This has been compared to those obtained in other host media, being higher than most of the microparameters reported in the literature.

The high transfer efficiencies obtained indicate that nonradiative energy transfer can be used to increase the number of pump channels of Yb^{3+} lasers in YAB by co-doping with Nd^{3+} ions. This good perspective together with the excellent laser and nonlinear properties of Yb^{3+} doped YAB crystals make the Nd^{3+};Yb^{3+}:YAB system a promising candidate to develop diode pumped lasers sources tunable in the UV-blue by means of sum frequency mixing processes involving pump and laser radiations. In this respect, all the parameters characterizing the $Nd^{3+} \rightarrow Yb^{3+}$ energy transfer given in this work are essential for a future modeling and optimization of this laser system.

ACKNOWLEDGMENTS

This work was carried out in the frame of a Spain-Italy Integrated Action cooperative project. This work has been supported by the Comunidad Autónoma de Madrid (CAM) under Project Nos. 07M/0065/2001 and 07N/0020/2002 and by the Comisión Interministerial de Ciencia y Tecnología (CICYT) under Project No. MAT2001-0167. The authors gratefully thank Erica Viviani (DST, Univ. Verona) for expert technical assistance. D. Jaque thanks the Ministerio de Ciencia y Tecnologia of Spain for a Ramon y Cajal contract.

[1] C. Hönninger, F. Morier-Genoud, M. Moser, U. Keller, L. R. Brovelli, and C. Harder, Opt. Lett. **23**, 126 (1998).
[2] C. Hönninger, G. Zhang, U. Keller, and A. Giesen, Opt. Lett. **20**, 2402 (1995).
[3] A. A. Kaminskii, *Crystalline Lasers: Physical Processes and Operating Schemes* (Chemical Rubber Corp., Boca Raton, FL, 1996).
[4] W. Koechner, *Solid State Laser Engineering* (Springer, Berlin, 1999).
[5] T. Y. Fan, IEEE J. Quantum Electron. **29**, 1457 (1993).
[6] Y. Guyot, H. Manaa, J. Y. Rivoire, R. Moncorge, N. Garnier, E. Descroix, M. Bon, and L. Laporte, Phys. Rev. B **51**, 784 (1995).
[7] E. Montoya, J. Capmany, L. E. Bausa, T. Kellner, A. Diening, and G. Huber, Appl. Phys. Lett. **74**, 3113 (1999).
[8] D. A. Hammons, J. M. Eichenholz, Q. Ye, B. H. T. Chai, L. Shah, R. E. Peals, M. Richardson, and H. Qiu, Opt. Commun. **156**, 327 (1998).
[9] F. Mougel, K. Dardenne, G. Aka, A. Kahn-Harari, and D. Vivien, J. Opt. Soc. Am. B **16**, 164 (1999).
[10] P. Wang, J. M. Dawes, P. Dekker, D. S. Knowles, J. A. Piper, and B. S. Lu, J. Opt. Soc. Am. B **16**, 63 (1999).
[11] D. Jaque, J. Capmany, and J. García Solé, Appl. Phys. Lett. **75**, 325 (1999).
[12] D. Jaque, J. Capmany, F. Molero, and J. García Solé, Appl. Phys. Lett. **73**, 3659 (1998).
[13] D. Jaque and J. J. Romero, J. Appl. Phys. **90**, 1070 (2001).
[14] P. Dekker, J. M. Dawes, J. A. Piper, Y. Liu, and J. Wang, Opt. Commun. **195**, 431 (2001).
[15] P. A. Burns, J. M. Dawes, P. Dekker, J. A. Piper, J. Li, and J. Wang, Opt. Commun. **207**, 315 (2002).
[16] J. Bartschke, R. Knappe, K.-J. Boller, and R. Wallenstein, IEEE J. Quantum Electron. **33**, 2295 (1997).
[17] P. Wang, P. Dekker, J. M. Dawes, J. A. Piper, Y. Liu, and J. Wang, Opt. Lett. **25**, 731 (2000).
[18] E. L. Belokoneva, A. V. Azizov, N. I. Leonyuk, M. A. Simonov, and N. V. Belov, Zh. Strukt. Khim. **22**, 196 (1981).
[19] D. Jaque, J. Capmany, Z. D. Luo, and J. García Solé, J. Phys.: Condens. Matter **9**, 9715 (1997).
[20] P. Wang, J. M. Dawes, P. Dekker, and J. A. Piper, Opt. Commun. **174**, 467 (2000).
[21] D. Jaque, J. Capmany, J. García Solé, Z. D. Luo, and A. D. Jiang, J. Opt. Soc. Am. B **15**, 1656 (1998).
[22] D. Jaque, J. Opt. Soc. Am. B **19**, 1326 (2002).
[23] M. H. Bartl, K. Gatterer, E. Cavalli, A. Speghini, and M. Bettinelli, Spectrochim. Acta, Part A **57**, 1981 (2001).
[24] M. J. Weber, Phys. Rev. B **4**, 3153 (1971).
[25] D. F. Sousa, F. Batalioto, M. J. V. Bell, S. L. Oliveira, and L. A. O. Nunes, J. Appl. Phys. **90**, 3308 (2001).
[26] D. L. Dexter, J. Chem. Phys. **21**, 836 (1953).
[27] R. L. Orbach, *Optical Properties of Ions in Solids: Relaxation and Energy Transfer*, edited by B. DiBartolo (Plenum, New York, 1975).
[28] B. Henderson and G. F. Imbusch, *Optical Spectroscopy of Inorganic Solids* (Oxford Science Publications, Oxford, Clarendon, 1989).
[29] D. Jaque, J. A. Muñoz, F. Cussó, and J. García Solé, J. Phys.: Condens. Matter **10**, 7901 (1998).
[30] G. E. Peterson and P. M. Bridenbaugh, J. Opt. Soc. Am. **54**, 644 (1964).
[31] E. J. Sharp and J. E. Miller, J. Appl. Phys. **40**, 4680 (1969).
[32] J. E. Miller and E. J. Sharp, J. Appl. Phys. **41**, 4718 (1970).
[33] Z. D. Luo, Prog. Nat. Sci. **4**, 504 (1994).
[34] D. Jaque, J. Capmany, J. Rams, and J. García Solé, J. Appl. Phys. **87**, 1042 (1999).
[35] D. Jaque and J. García Solé, Chem. Phys. Lett. **334**, 309 (2001).
[36] R. Reisfeld and Y. Kalisky, Chem. Phys. Lett. **80**, 178 (1981).
[37] W. Ryba-Romanowski, S. Golab, L. Cichosz, and B. Jezowska-Trzebiatowska, J. Non-Cryst. Solids **105**, 295 (1988).
[38] M. J. Weber, Phys. Rev. B **4**, 2932 (1971).
[39] M. V. Artamonova, Ch. M. Briskina, L. D. Zusman, and A. G. Skeleznev, Sov. Phys. JETP **35**, 457 (1972).
[40] Yu. K. Voronko, V. V. Osiko, and I. A. Scherbakov, Izv. Akad. Nauk SSSR, Ser. Fiz. **46**, 970 (1981).
[41] M. Inokuti and F. Hirayama, J. Chem. Phys. **43**, 1978 (1965).
[42] T. Förster, Z. Naturforsch. A **4A**, 321 (1949).
[43] C. Parent, C. Lurin, G. Le Flem, and P. Hagenmuller, J. Lumin. **36**, 49 (1986).
[44] C. Lurin, C. Parent, G. Le Flem, and P. Hagenmuller, J. Phys. Chem. Solids **46**, 1083 (1985).